Aus der Klinik III für Innere Medizin, Kardiologie
der Universität zu Köln
Direktor: Universitätsprofessor Dr. med. Stephan Baldus

Activation of Endothelial Cells and Immune cell infiltration in the murine Marfan Syndrome depending on Myeloperoxidase deficiency

Inaugural-Dissertation zur Erlangung der Doktorwürde
der Medizinischen Fakultät
der Universität zu Köln

vorgelegt von
Jil Bastigkeit
aus Ahlen

promoviert am 26. Mai 2025

Gedruckt mit Genehmigung der Medizinischen Fakultät der Universität zu Köln

Druckjahr 2025

Dekanin/Dekan: Universitätsprofessor Dr. med. G. R. Fink
1. Gutachter: Universitätsprofessor Dr. med. S. Baldus
2. Gutachter: Universitätsprofessor Dr. rer. nat. G. F. Sengle

Erklärung

Ich erkläre hiermit, dass ich die vorliegende Dissertationsschrift ohne unzulässige Hilfe Dritter und ohne Benutzung anderer als der angegebenen Hilfsmittel angefertigt habe; die aus fremden Quellen direkt oder indirekt übernommenen Gedanken sind als solche kenntlich gemacht.

Bei der Auswahl und Auswertung des Materials sowie bei der Herstellung des Manuskriptes habe ich Unterstützungsleistungen von folgenden Personen erhalten:

Herr Dr. Dennis Mehrkens
Frau Lauren DeVore

Weitere Personen waren an der Erstellung der vorliegenden Arbeit nicht beteiligt. Insbesondere habe ich nicht die Hilfe einer Promotionsberaterin/eines Promotionsberaters in Anspruch genommen. Dritte haben von mir weder unmittelbar noch mittelbar geldwerte Leistungen für Arbeiten erhalten, die im Zusammenhang mit dem Inhalt der vorgelegten Dissertationsschrift stehen.

Die Dissertationsschrift wurde von mir bisher weder im Inland noch im Ausland in gleicher oder ähnlicher Form einer anderen Prüfungsbehörde vorgelegt.

Die dieser Arbeit zugrunde liegenden Rohdaten der Intravitalmikroskopie wurden ohne meine Mitarbeit im Labor des Universitätsklinikums Düsseldorf im Cardiovascular Research Laboratory der Gruppe Cardiovascular Immune Biology ermittelt. Die Analyse der Datensätze habe ich eigenständig durchgeführt.

Erklärung zur guten wissenschaftlichen Praxis:

Ich erkläre hiermit, dass ich die Ordnung zur Sicherung guter wissenschaftlicher Praxis und zum Umgang mit wissenschaftlichem Fehlverhalten (Amtliche Mitteilung der Universität zu Köln AM 132/2020) der Universität zu Köln gelesen habe und verpflichte mich hiermit, die dort genannten Vorgaben bei allen wissenschaftlichen Tätigkeiten zu beachten und umzusetzen.

Köln, den 10.02.2025

Unterschrift: .....

Widmung

Table of contents

Abbreviations and Akronyms

A	Ampere
AAA	Abdominal aortic aneurysm
Acta2	actin alpha 2
ANOVA	Analysis of variance
ARB	Angiotensin receptor blocker
BCA	Bicinchonic acid
BSA	Bovine serum albumin
BW	Body weight
CCL	CC-chemokine ligand
Cdh5	Cadherin 5
Cldn5	Claudin 5
Ctla2a	cytotoxic T-lymphocyte antigen 2 alpha
CVD	Cardiovascular Disease
Cxcl	Chemokine (C-X-C motif) ligand
DALY	disability-adjusted life years
DAPI	4',6-Diamidino-2-phenylindole, Dihydrochloride
DKO	Double Knockout
DMSO	Dimethylformamid
DTT	Dithiothreitol
EC	Endothelial cells
ECL	enhanced chemiluminescence
ECM	Extracellular matrix
EndMT	Endothelial-to-mesenchymal transition
ERK	Extracellular-signal related kinase
Esam	Endothelial cell adhesion molecule
Fabp4	Fatty acid binding protein 4
Fbn1	Fibrillin 1
FBS	fetal bovine serum
GAPDH	Glyceraldehyde-3-phophate dehydrogenase
H_2O_2	Hydrogen peroxide
HOCl	Hypochlorous acid
ICAM-1	Intercellular adhesion molecule 1
IF	Immunofluorescence
IL	Interleukin
Itga8	Integrin Subunit alpha 8
JNK	C-Jun N-terminal kinase

kDa	kilodalton
Lyve1	Lymphatic vessel endothelial hyaluronan receptor-1
Ly6G	Lymphocyte antigen 6 complex locus G6D
M	molar mass
MAPK	p38 mitogen-activated protein kinase
mL	milliliter
MFS	Marfan Syndrome
MMP	Matrix metalloproteinase
MPO	Myeloperoxidase
Myl9	Myosin Light Chain 9
Ncam1	neural cell adhesion molecule 1
NCBI	National Center for Biotechnology
NO	Nitric Oxide
Nts2	Neurotensin receptor 2
PBS	Phosphate buffered saline
Pecam1	Platelet and endothelial cell adhesion molecule 1
PFA	Paraformaldehyde
PMN	Polymorphonuclear neutrophil
PRKG	protein kinase cGMP-dependent
ROS	Reactive Oxygen Species
scRNAseq	Single Cell Ribonucleic acid Sequencing
SEM	Standard error of mean
sGC	soluble guanlylate cyclase
SMAD	Suppressor of mothers against decapentaplegic
SRA	Sequencing Read Archive
TAA	Thoracal Aortic Aneurysm
Tagln	Transgelin
TBS-T	Tris-buffered saline with Tween20
TGF-β	Transforming Growth Factor beta
Tie-1	Tyrosine kinase with immunglobuline-like and EGF-like domains 1
V	Volt
VCAM-1	Vascular call adhesion molecule 1
Vcan	Versican
VSMC	Vascular Smooth Muscle Cell
vWF	von Willebrand factor
YLL	Years of life lost
µL	Microliter
µM	Micromolar

1. Abstract

Marfan Syndrome (MFS) is a genetic disorder caused by a mutation in the fibrillin 1 (Fbn1) gene leading to various phenotypical alterations, like long bone overgrowth and ocular lens dislocation. Aortic root aneurysm formation is the major cause of death due to subsequent dissection or rupture. Current treatment options include betablockers and Losartan, which do not show sufficient attenuation of aneurysm formation, leaving open heart aortic root replacement surgery as only therapy. Myeloperoxidase (MPO), a protein abundant predominantly in neutrophils, has been found to play a role in the pathomechanism of aortic wall degeneration and subsequent aneurysm formation. Using in vivo murine disease models, MPO has been elucidated to not only activate but alter endothelial cells (EC) as well as to increase inflammatory responses. In MPO deficient MFS mice a lower intercellular adhesion molecule 1 (ICAM-1) expression on ascending aortic EC has been observed using immunofluorescence staining, as well as less leukocyte rolling, adhesion, and infiltration in peripheral vessels as demonstrated by intravital microscopy. In addition, inflammatory pathways have been found to be upregulated in MFS EC, as shown by scRNAseq. Further a cluster of ECs resembling lymphatic ECs strengthens the hypothesis that inflammatory processes play a major role in MFS pathogenesis. MPO appears to be a driving factor of inflammation in MFS aneurysm formation and therefore may be of therapeutic interest.

1.1 Zusammenfassung in deutscher Sprache

Das Marfan Syndrom ist eine autosomal-dominant vererbte Mutation im Fibrillin-1-Gen, die zu unterschiedlichen phänotypischen Ausprägungen führt. Aortenwurzelaneurysmen mit nachfolgender Dissektion oder Ruptur stellen die Haupttodesursache und das lebenszeitverkürzende Problem dar. Aktuelle medikamentöse Therapieoptionen mit ß-Blockern und Losartan vermindern zwar das Aneurysmawachstum, jedoch bleibt die Aortenwurzelersatzoperation die einzig kurative Therapie.

Myeloperoxidase, ein Protein, dass vorrangig in neutrophilen Granulozyten vorkommt, wird in verschiedenen Pathomechanismen kardiovaskulärer Erkrankungen, wie z.B. der Degeneration der Aortenwand, diskutiert. Mit Hilfe von in vivo Mausmodellen kann gezeigt werden, dass MPO einen Einfluss auf die Endothelzellen hat, der sich in deren Aktivierungszustand und ihrer Genexpression widerspiegelt. MPO-defiziente MFS Mäuse zeigen eine geringere ICAM-1 Expression in der aufsteigenden Aorta, sowie eine geringere Leukozytendiapedese in peripheren Arterien, wie intravitalmikroskopisch gezeigt werden kann. Dies beweist eine geminderte Immunantwort in MPO-defizienten MFS Mäusen. In einer single-cell RNA sequencing Analyse konnte gezeigt werden, dass inflammatorische Signalwege in MFS Endothelzellen im Vergleich zu Wildtypzellen hochreguliert sind, was

darauf hindeutet, dass aktivierte Endothelzellen und Entzündungsreaktionen zum Aneurysmawachstum beitragen. Es waren zwei Untergruppen der Endothelzellen zu identifizieren, einer ähnelt in seinem Expressionsmuster den lymphatischen Endothelzellen, was weiter auf inflammatorische Prozesse hinweist.

2. Introduction

2.1 Cardiovascular Disease

Cardiovascular disease (CVD) is the leading cause of death, accounting for 32% of all deaths worldwide, e.g. in both low- and high-income countries.[1,2] It has been causing an increase of the number of years of life lost (YLL), as well as the disability-adjusted life years (DALY), contributing to rising disability and healthcare costs for decades.[2] CVD includes a range of diseases affecting the heart and blood vessels, such as hypertension and coronary heart disease.[3]

2.1.1. Aortic aneurysm

Aortic aneurysms account for 1-2% of all deaths in industrialized countries.[4] Defects in the extracellular matrix (ECM), mainly in the medial layer of the vessel wall, cause enlargement of arteries, defined and categorized by their diameter.[4,5] The definition of aneurysms requires a 50% increase of normal diameter in relation to body size and age.[6] Enlarged arteries are predisposed to dissection or rupture, resulting in a 50% sudden death rate.[7] While abdominal aortic aneurysms (AAA) are associated with degeneration such as age or atherosclerosis, thoracic aortic aneurysms (TAA) are strongly associated with genetic disorders.[4,8] TAA are further characterized by their exact localization such as root, ascending aorta, and aortic arch.[9] TAA usually remains asymptomatic until its complications cause symptoms.[10] Aortic aneurysms are associated with increased matrix metalloproteinases (MMP) production leading to wall remodeling and immune cell recruitment.[11] An additional major component in the pathogenesis of TAA is the vascular smooth muscle cell (VSMC) phenotypic switch from contractile to synthetic.[12] Under physiological conditions, VSMC regulate vascular tone and diameter through contraction and dilatation, while synthetic VSMC show increased proliferation and migration and less proteins involved in contraction.[13]

2.2 Marfan Syndrome

2.2.1 Genetics and clinical presentation

Marfan Syndrome is the most common inherited connective tissue disorder with a prevalence of 1 in 5000 individuals.[14] The disease is predominantly inherited as an autosomal dominant trait and therefore has no gender specificity, yet 30% of MFS patients develop it as a result of a de novo mutation.[15] Typical clinical manifestations of MFS include aortic root dilatation, skeletal long bone overgrowth, scoliosis and ocular lens dislocation, the main cause of death being TAA and subsequent aortic dissection or rupture.[16] MFS is caused by several different

mutations, primarily found in the Fbn1 gene on chromosome 15q21.1, encoding the ECM protein fibrillin-1.[17] Fbn1 is a 350 kDa cysteine-rich glycoprotein primarily responsible for structuring the extracellular microfibrils and elastic fibers, which both play an important role in the stability of vessels.[18,19,20]

2.2.2 Pathophysiology

Aortic dysfunction in MFS is manifested primarily in the media of the aortic wall by elastic matrix abnormalities, elastin loss and VSMC alterations.[21,22] Several causes leading to elastin fiber fragmentation are known. Besides the previously described mutation in the Fbn1 gene, there is evidence that the transforming growth factor-β (TGF-β) is altered in its activation and bioavailability by the extracellular matrix. Both canonical (SMAD-dependent) and non-canonical (ERK, JNK, and MAPK-dependent) TGF-β signaling pathways promote TAA formation.[23,24,25] Extracellular-signal related kinase 1/2 (ERK1/2) inhibition has been shown to reduce aneurysm growth in murine MFS.[26] Smads are transcriptional factors that are the main signal transducers of the TGF-β-signaling pathway, ultimately leading to expression regulation of genes such as MMP and plasminogen activator inhibitor 1 (PAI-1).[27] A correlation between elastin strand breaks and a higher level of matrix metalloproteinases (MMP) has been observed in MFS.[28,29] Elevated levels of nitric oxide (NO), mediated by soluble guanlylate cyclase protein kinase cGMP-dependent (sGC-PRKG) signaling, lead to aortic wall degeneration.[30] Accumulation of reactive oxygen species (ROS), such as NO and hydrogen peroxide (H_2O_2), lead to oxidative stress and subsequent vascular damage.[31] Due to downregulated Akt/eNOS-induced NO production, endothelium-dependent relaxation in MFS appears to be impaired, resulting in increased vascular tone.[32] Increased levels of ROS in affected aortic segments have been explained by an increased NAPDH activity and angiotensin II.[33]

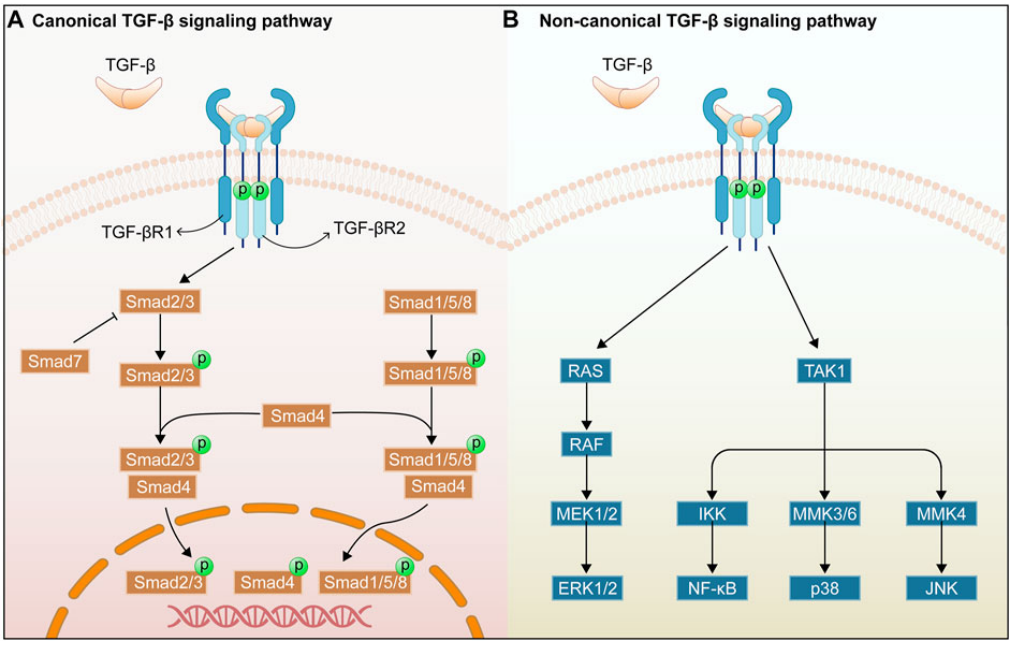

Figure 1 *Non-canonical and canonical TGF-β-signaling pathways*[34]

(1) Immune response

Accumulating evidence suggests that inflammation occurs early on in the disease and correlates with the severity of aortic root dilatation.[35] Elevated numbers of $CD4^+$ T-helper cells in the media and $CD8^+$ T cells in the adventitia,[36] B-lymphocytes and macrophages in the media of TAA have been found in patients with MFS.[37] Macrophage chemotaxis is stimulated by recombinant FBN-1 fragments and aortic extracts in both mice and humans, suggesting that leukocyte infiltration may account for disease progression in MFS.[38,39] The role of the immune system in the pathogenesis of MFS pathogenesis is largely unknown.

(2) Myeloperoxidase

Myeloperoxidase (MPO) is a proinflammatory heme peroxidase stored mainly in neutrophil granulocytes, accounting for 5% of their dry mass, and to a lesser extent in monocytes.[40] MPO is involved both in host defense as well as in the pathogenesis of inflammatory vascular diseases such as atherosclerosis.[41] Host defense is mediated by various mechanisms. MPO enables the transcytosis of neutrophils through the endothelium into the extravascular space, mainly through electrostatic forces due to its cationic charge.[42] In the subendothelial space MPO colocalizes with fibronectin, a protein of the extracellular matrix. Together with nitrotyrosine it alters the quaternary structure of the ECM-molecule leading to ECM alterations that contribute to tissue damage.[43,44] The reactions of MPO can be roughly divided into two reaction cycles involving two catalytic compounds. In the halogenation cycle, Compound I reacts with chloride and hydrogen peroxide (H_2O_2) to form hypochlorous acid (HOCl), leading to further chlorination and oxidation processes important for neutrophil microbicidal activity.

During the peroxidase cycle Compound I is reduced to Compound II by losing an electron during oxidation of organic substrates. It generates reactive molecules such as tyrosyl radicals and highly reactive nitrogen dioxide, leading to nitration of protein residues, lipid peroxidation, and the formation of nitrotyrosine, a marker of oxidative stress and inflammatory tissue. [45,46] MPO has been associated with several cardiovascular diseases. By lowering the NO availability through reduced activity of the endothelial NO synthase, MPO enhances endothelial dysfunction.[47] It has been shown to promote TAA formation in a murine MFS model by affecting ROS production in the aortic wall, activating matrix degrading enzymes and inducing VSMC apoptosis and elastin defragmentation.[48,33] Serum MPO levels have been shown to correlate with endothelial dysfunction and mortality in cardiovascular disease in humans.[49,50] Further, MPO is associated with abdominal aortic aneurysm as well as intracranial aneurysms.[51,52] MPO inhibition appears to attenuate inflammation and tissue degeneration, making it a promising therapeutic target.[53] The vast majority of MPO-deficient patients show no clinical symptoms except a decreased ability to combat fungal infections.[54]

2.3 Treatment

Treatment of MFS can be divided into surgical and non-invasive therapies. Medical therapies consist of β_1-receptor blockers[55] or the angiotensin-II-receptor antagonist (ARB) Losartan. Losartan attenuates TGF-β-related pathways and reduces TAA growth in MFS patients to the same extent as β_1-receptor blockers.[56,24] It also lowers systemic blood pressure, which is beneficial in patients with aortic aneurysms.[24] While these medical options are slowing the growth of TAA, the only treatment preventing premature death is surgical repair.[57]

2.4 Endothelial cells

Endothelial cells (EC) line the vasculature and are connected by adherens and tight junctions.[58] EC serve as the communication layer between blood flow and vessel media.[59] They obtain various functions for vessel function and homeostasis. EC are driving immune cell extravasation by expression of adhesion molecules, chemoattractants and other cell surface interleukins and proteins, like e.g. intercellular adhesion molecule 1 (ICAM-1) and vascular cell adhesion protein 1 (VCAM-1).[60,61] Further, they are able to directly influence vascular tone of VSMC by endothelial NO synthase (eNOS).[59,62]

2.4.1 Endothelial cells in aortic aneurysm

While the role of VSMC in aneurysm formation is largely understood, the role of EC remains to be unraveled further. Blood flow turbulences cause endothelial alterations, leading to apoptosis, proliferation, increased permeability and immune cell infiltration and adhesion.[59,62] Dysregulated eNOS leads to an increase of ROS and oxidative stress in the media and subsequently helps aneurysm formation.[59] Endothelial-to-mesenchymal transition (EndMT) is driven by TGF-β signaling, oxidative stress and inflammatory cytokines. EndMT describes the shift in the expression pattern of EC, leading to a phenotypic expression of SMC markers and subsequent increasing permeability of endothelium.[11] Furthermore, the loss of tight junctions appears to play a role in TAA formation.[63]

2.4.2 Lymphatic endothelial cells

Lymphatic ECs are amongst the first cells in contact with inflammatory molecules and are important in controlling communication with immune cells, being able to alter the immune response by expression of cytokines, adhesion molecules and regulation of transport functions.[64] They synthesize CC-chemokine ligand 21(CCL21), a chemoattractant, pro-inflammatory chemokines, and growth factors.[65]

2.5 Question and aim of work

Considering the above facts, especially the lack of a sufficiently effective causal treatment for MFS patients regarding TAA formation and thus the increased risk of aortic dissection, this project attempts to find a possible drug target to inhibit TAA formation and growth. Considering the inflammatory immune response and the consecutive alteration of the ECM in the aorta, MPO is thought to be a driving factor and thus to be investigated further. Therefore, this project seeks to elucidate the role of MPO in the progression of MFS aneurysms, with a focus on

endothelial alterations and immune response. The hypothesis is that MPO drives the inflammatory response in MFS, thereby promoting TAA growth.

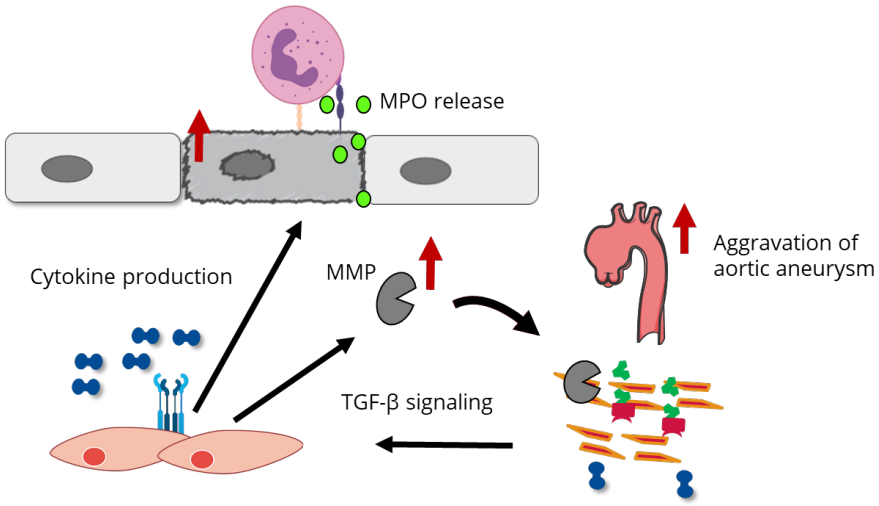

Figure 2 *MPO affecting aneurysm formation hypothesis*

Binding of leukocytes to endothelium bound adhesion molecules leads to MPO release into the aortic wall. MPO leads to production of ROS and intensifies the inflammatory response resulting in increased adhesion molecule production, and thereby increased leukocyte diapedesis. Endothelial cells are activated and altered. The activation of MMPs, and the TGF-β signaling pathway leads to the destruction of ECM.

3. Material and Methods

3.1 Material

3.1.1 Mouse model

Heterozygous $Fbn1^{C1041G/+}$ (MFS) mice with a missense mutation in the Fbn1 gene (glycine for cysteine substitution at position 1041) on C57BL/6J background were purchased from Jackson Laboratory (#:012885) and were crossed with MPO-deficient mice ($MPO^{-/-}$) in the animal facility of the University of Cologne to obtain MPO-deficient MFS mice ($MFSxMPO^{-/-}$). Wild type (WT) and MPO-deficient littermates were analyzed as controls. Animals were maintained according to institutional guidelines, and all experiments approved by the local Animal Care and Use Committees (Ministry for Environment, Agriculture, Conservation and Consumer Protection of the State of North Rhine-Westphalia: State Agency for Nature, Environment and Consumer Protection (LANUV), NRW, Germany, AZ: 84-02.04.2019.A033) and conformed to the guidelines from Directive 2010/63/EU of the European Parliament on the protection of animals used for scientific purposes. Male mice were sacrificed at 12 weeks for tissue dissection and further processing. Therefore, mice were deeply anaesthetized by isoflurane inhalation (Isofluran-Piramal®, Piramal Critical Care, Voorschoten, The Netherlands; 5% vol/vol for induction and 2% vol/vol for maintenance of anaesthesia) and subcutaneous injection of buprenorphine (TEMGESIC®, Indivior Europe Limited, Dublin, Ireland; 0.1 mg per kg body weight). Pedal reflex testing was used to confirm adequate anesthesia and mice were euthanized by cardiac exsanguination.

3.1.2 Antibodies

Antibody	**Species**	**Dilution**	**Product information**
Anti-Ly6G	rat	1:200	Abcam, AlexaFluor 594, ab307167
Anti-ICAM-1	hamster	1:200	Invitrogen, MA5405
Anti-vWF	mouse	1:100	Dako, A0082
Anti-MPO	rabbit	1:200	Calbiochem, 475915
Anti-Nitrotyrosine	goat	1:300	LSBioSciences, LS-C124272
Anti-Fibronectin	mouse	1:50	Sigma Aldrich, f0791
DAPI		1:1000	Thermo Fischer, D1306
Anti-GAPDH	rabbit	1:10000	Cell Signaling, 2118
Anti-pERK 1/2	rabbit	1:1000	Cell Signaling, 9101
Anti-ERK 1/2	rabbit	1:1000	Abcam, 209321

Anti-NOX2	rabbit	1:1000	Abcam, 129068
Anti-NOS2	rabbit	1:1000	Abcam, ab15323
Anti-pSMAD2	rabbit	1:1000	Cell Signaling, 18338
Anti-SMAD2/3	rabbit	1:1000	Abcam, ab71109
Anti-TGF-ß receptor 1	rabbit	1:200	Santa Cruz, sc-399
Anti-TGF-ß receptor 2	rabbit	1:1000	Abcam, ab186838
Anti-Cleaved caspase 3	rabbit	1:1000	Cell Signaling, 9661

Secondary Antibody	**Species**	**Dilution**	**Product Information**
Anti-rat Alexa 594	rat	1:50	Invitrogen, a11007
Anti-Hamster Cy3	goat	1:200	Dianova, 127-165-099
Anti-Mouse Alexa Fluor 488	chicken	1:500	Invitrogen, A21200
Anti-rabbit Alexa Fluor 488	goat	1:500	Abcam, ab150077
Anti-rabbit, HRP	goat	1:10000	Invitrogen, 31460

Isotype Controls	**Product information**
Rat IgG isotype	Invitrogen 31933
Armenian Hamster IgG isotype	Invitrogen, 14-4888-8
Goat IgG isotype	Invitrogen, 02-6202

3.1.3 Consumables

Product	**Manufacturer**	**Article number**
Sterile pipette tips:		
0,5-20µl	Biosphere	70.1116.210
20 µl	SurPhob	VT0220
2-100 µl	Biosphere	70.760.212
2-200 µl	Biosphere	70.760.21
1250 µl	SurPhob	VT0270
Serological pipettes:		
5 ml	Greiner Bio-One, Kremsmünster	606 180
10 ml	Greiner Bio-One, Kremsmünster	607 180
25 ml	Greiner Bio-One, Kremsmünster	760 180
50 ml	Greiner Bio-One, Kremsmünster	760 180
Cuvette	Sarstedt, Nümbrecht	67.742
Scalpel	Feather Safety Razor	02.001.30.015cv
Reaction vials:		

1,5 ml	Sarstedt, Nümbrecht	72.706.400
2 ml	Sarstedt, Nümbrecht	72.659.400
5 ml	Eppendorf, Hamburg	EP0030122321
12-Well Plate	Sarstedt, Nümbrecht	83.3921
Gloves	Remesco, Wien	D1502-17
Falcons:		
15 ml	Greiner Bio-One, Kremsmünster	188 271-N
50 ml	Greiner Bio-One, Kremsmünster	27/261
Filter 22 µm	Sartorius, Göttingen	17846-ACK
Chamber slide	Thermo-Fisher, Waltham	143361
Cover glass	Th. Geyer, Renningen	7695031
Filter paper	Carl Roth, Karlsruhe	CL75.1
Syringe 1ml	BD, Madrid	303172
Syringe 50ml	Braun, Melsungen	4617509F
Cannula	BD, Madrid	304434
Blades for Cryotom	EMS, Hatfield	71960
Destruction bag	Sarstedt, Nümbrecht	86.1197
Cryovials	VWR, Radnor	479-1375
Precellys 0,5ml	Bertin, Rockville, US	P000933-LYSK0-A
Protein Gels	BioRad Laboratories Germany	4561034

3.1.4 Devices

Product	Manufacturer	Article number
pH-measuring	Mettler Toledo, Columbus	30266626
Thermomixer	Eppendorf, Hamburg	5382000015
Centrifuge Eppendorf 5810R	Eppendorf, Hamburg	5811000015
Plate Reader	Thermo Fischer, Waltham	11590685
Homogenizator	Bertin Instruments, Montigny-le. Bretonneux, France	P000669PR240A
Cell Counter	BioRad, Hercules	1450102
NanoDrop	Thermo Fischer, Waltham	ND-ONE-
Digital microscope	Keyence, Osaka, Japan	BZ-X810
Trans-Blot Turbo	BioRad, Hercules, USA	690BR031130
Fusion FX, Western Blot Imager	Vilber, Collégien, France	12200866
Nitrogen Tank	Harsco, Husum	CFE-160/280
Intravital microscope	Leica Microsystems, Germany	DM6 FS

3.1.5 Chemicals

Product	Manufacturer	Article number
TRIS Base	Carl Roth, Karlsruhe	AE15.2
Tween 20	Sigma-Aldrich, St. Louis	P7949
Triton X-100	Thermo Fischer, Waltham	85111
PBS tablets	Thermo Fischer, Waltham	18912-012
PBS sterile	Thermo Fischer, Waltham	10010-023
Running buffer	Novex	LC2675
Transfer buffer	BioRad, Hercules	10026938
NaCl 0,9%	Fresenius Kabi, Bad Homburg	B240423
BSA	Carl Roth, Karlsruhe	8076.3
Femto	Thermo-Fisher, Waltham	34096
ECL	GE Healthcare, Chicago	RPN2106
Glycin	PanReac, Schaffhausen	A1067,1000
EDTA 0,5 M pH 8	PanReac, Schaffhausen	A4892,0500
SDS 20%	PanReac, Schaffhausen	A0675,0500
IGEPAL	Sigma-Aldrich, St. Louis	CA-630
Acetone	Chem Solute, Roskilde	2654.2500
Ethanol absolut	Chem Solute, Roskilde	2246.1000

Ethanol 70%	Otto Fischar, Saarbrücken	707 1074
Hydrochloric acid 37%	Carl Roth, Karsruhe	9277.1
Isoflurane	Priamal, Voorschoten	09714675
Tissue-Tek	Sakura, Alphen aan den Rijn	4583
Trizol	Quiagen, Hilden	79306
Protease-Inhibitor	Roche, Basel	04693159001
Phospho Stop	Roche, Basel	4906845001
Dithiothreitol (DTT)	Sigma-Aldrich, St. Louis	43816
Nitrocellulose membranes	Cytiva, Marlborough, USA	10600001
Ampuwa	Fresenius Kabi, Bad Homburg	1088811
Ponceau-S	Sigma-Aldrich, St. Louis	P7170
Fluorescence Mounting medium	Dako	S3023
Vascular Cell Basal Medium	ATCC, Virgina	PCS-100-030
VSMC Growth Kit	ATCC, Virgina	PCS-100-042
Human AoSMC	Bioscience, Lonza	CC-2571
Prestained protein marker	Thermo Scientific	PL00001
Calibration solutions		
pH 10,01	Hanna Instruments	HI70010P
pH 7,01	Hanna Instruments	HI70007P
pH 4,01	Hanna Instruments	HI70004P

3.1.6 Kits

Product	**Manufacturer**	**Article number**
Pierce BCA-Protein-Assay Kit	Thermo-Fisher, Waltham, USA	23225
SuperSignal™ West Femto Maximum Sensitivity Substrat	Thermo-Fisher, Waltham USA	34094
Amersham™ ECL™ Western Blotting Detection Reagents	GE Healthcare, Little Chalfont, UK	RPN2106
TrueVIEW® Autofluorescence Quenching Kit	Vector, Burlingame, USA	SP-8400

3.1.7 Buffer

	RIPA Buffer
Tris-HCl	50mM

NaCl	150mM
Igepal	1%
Na-Desoxychalat	0,5%
SDS	0,1%
EDTA	1mM
Glycerol	10%
pH	7,5

Table 1 *RIPA buffer for protein isolation of aortic tissue*

Per 15ml RIPA-buffer 1 phosphatase and protease inhibitor-pill by Roche was added.

	10x TBS	10x TBS-T
Tris Base	0,5M	0,5M
NaCl	1,5M	1,5M
Tween 20	-	0,1%
pH	7,5	7,5

Table 2 *TBS and TBST buffer for Western Blot Analysis*

	4x Lämmli
Tris Base	126mM
Glycerol	40%
SDS	8%
Bromophenol Blau	0,04%
pH	6,8

Table 3 *4x Lämmli buffer for Western Blot Analysis*

To produce 4x Lämmli + DTT, DTT was mixed with 4x Lämmli 1:9.

3.2 Methods

3.2.1 Immunofluorescence (IF)

(1) Aortic Tissue

For histological preparation, mouse ascending aorta specimens were embedded in Tissue Tec, cryopreserved and stored at -80°C. Frozen 8 µm thick sections of the aortas were air dried at room temperature for 10 minutes before fixation in cold acetone for 10 minutes. Permeabilization was performed with 0.1% Triton-X-100 diluted in phosphate-buffered saline (PBS) for an additional 10 minutes before blocking specimens with blocking solution (3% bovine serum albumin (BSA) and 10% fetal calf serum in 1x PBS) for one hour at room temperature. Primary antibody diluted in blocking solution was incubated overnight at 4°C in a dark, humidified chamber. After several rinses in 0.02% Tween-20 in 1x PBS and pure 1x PBS alone, the tissues were incubated with the corresponding specific secondary fluorescent antibody diluted in blocking solution for one hour at room temperature and rinsed again. To obtain a better and more specific signal, samples were treated with Vector TrueVIEW reagents to quench autofluorescence signals, especially for staining with a fluorescence signal at 488nm, since elastic fibers emit an autofluorescence signal at this wavelength. For cell nuclei staining DAPI was used at 1/1000 dilution in PBS and incubated for 10 minutes at room temperature in a dark humidified chamber and rinsed again. Specimens were mounted using the Fluorescence Mounting medium and cooled for at least four hours before visualization. The specificity of the immunofluorescence staining was verified by the substitution of the specific primary antibody with the isotype IgG control as a negative control.

Images were visualized and captured using a Keyence BZ-X800 microscope (Keyence, Osaka, Japan) at 10x magnification for a view of the entire aortic section as well as at 40x magnification for detailed analysis. Sections were quantified using the Keyence BZ-II analyzer software or Fiji/ImageJ.

(2) ICAM-1

The Anti-ICAM-1 monoclonal antibody was used at a dilution of 1/200. For the negative control an Armenian Hamster IgG isotype control was processed in the same manner as the anti-ICAM-1 antibody. Goat IgG anti-Armenian Hamster Cy3 was used as the secondary fluorescent antibody at 1/200 dilution. An anti van-Willebrandt-Factor (vWF) antibody was used at 1/100 dilution as a localization reference, as it is considered an EC marker.[66]

Quantitative analysis was performed using Fiji/ImageJ.[67] Therefore, the IgG isotype negative controls were used to set the threshold for the validated specific signal and to exclude non-specific background noise. The positive signal of ICAM-1 was set in relation to the total endothelial area and compared between the four groups of mice.

(3) MPO, Ly6G

To demonstrate immune cell infiltration in the ascending aortic wall, sections were co-stained with an anti MPO antibody and a Ly6G antibody both diluted at 1/200 in 1x PBS. Isotype controls were treated equally. Images were used for representative purposes only and were not quantified.

3.2.2 Intravital Microscopy

Intravital microscopy was performed in collaboration with the AG Gerdes, Düsseldorf, Germany. Male, 10-14-week-old mice were anesthetized and injected with 100 mg/kg BW ketamine and 10 mg/kg BW xylazine i.p. for analgesia and placed on heating plate to avoid temperature drop. 100µl 0,1% Rhodamine 6G was injected via the tail to mark circulating leukocytes. After shaving of the scrotum, the cremaster muscle was detached from the external spermatic fasci and the exterior surface cleared from the connective tissue and pinned to a silicon board. The ventral side of the cremaster was incised from distal to proximal by thermocautery. For imaging, the pinned muscle was kept moist with 37°C warmed 0,9% sodium chloride. 60-second sequences of selected arterial vessels ranging in size between 30µm to 50µm were acquired on 5 different areas of the cremaster muscle. Intravital imaging was performed with a Leica DM6 FS microscope equipped with a DFC9000 GTC camera and a 25x saline-immersion objective. Image sequences were acquired with the LasX software (Leica) and analysis of leucocyte-endothelial cell interaction was performed with Fiji TrackMatev6.0.1[68] (Fiji/ImageJ).

3.2.3 Western Blot

(1) Homogenization

For protein isolation, ascending aortic specimens were mechanically lysed in RIPA Lysis Buffer and placed in homogenizator three times for 20 seconds each. They were then placed on ice for a 30 minute incubation before centrifugation for another 30 minutes at 4°C and 14.000g.

(2) Protein Assay

To determine the protein concentration, 10 µL of homogenized samples were prepared using the Pierce™ Bicinchonic acid (BCA) Protein Assay Kit according to instructions and placed into a plate reader.

(3) Gel electrophoresis

6µg of ascending aortic specimens, according to protein assay, were filled up to 30 µl with sterile distilled water and 10 µl 4x Laemmli buffer with Dithiothreitol (DTT). Samples were heated at 95°C for 10 minutes in a ThermoMixer, set back on ice and pipetted into gel. A prestained protein marker was added into one chamber of the gel for size reference. Running buffer was filled into the electrophoresis chambers. For alignment of samples, the electrophoresis was started at 60 Volt for 15 minutes, and then continued at 100 Volt.

(4) Blot

For transferal of the proteins onto a cellulose membrane, filter papers and membranes were soaked in SDS Transfer Buffer. Gel was transferred onto stack of two filter papers and the membrane and topped with another filter paper. To prevent bubbles, the stack was carefully pressed and rolled out. The Blot chamber was placed into TransBlot® Turbo™ Transfer System and run for 45 minutes at 2,5 mA, 10 V. For proof of a successful transferal the membrane was stained with Ponceau for two minutes and then rinsed with tris-buffered saline with 0.01% Tween20 (TBS-T).

(5) Antibody preparation and Evaluation

Membranes were blocked in blocking solution (5 % BSA in TBS-T) for one hour and incubated with primary antibodies diluted in blocking solution over night at 4°C at 1/1000 dilution. Samples were washed three times, ten minutes each, in TBS-T and then incubated with the secondary antibody at 1/10.000 dilution in blocking solution for one hour followed by another 30 minutes of washing. Samples were incubated with enhanced chemiluminescence (ECL) substrates for 30 seconds before visualization. For image capture, the Fusion FX (Peqlab) was used. Quantification was performed with Fiji/ImageJ. All results have been standardized with GAPDH as a reference protein.

(6) Stripping

For stripping the cellulose membranes of the antibodies, they were firstly washed with destillled water for 5 minutes and then incubated with 0.2 M NaOH for 3 minutes. Subsequently samples were washed with distilled water and TBS-T for five minutes each.

3.2.4 In-silico single-cell RNA sequencing

(1) NCBI SRA accession

To investigate changes in the expression profile of EC populations between WT and MFS mice we examined data sets of murine aortic tissue from both WT and MFS obtained by Pedroza et al.[69] They sacrificed mice at 4 and 24 weeks of age for aortic tissue digestion, followed by single-cell RNA sequencing (scRNAseq) at the Stanford Genome Sequencing Service Center. Samples were targeted at 5000 cells for sequencing and processed on a 10X Genomics microfluidics chip to generate barcoded gel bead-in emulsions (GEM). scRNAseq was performed on an Ilumina HiSeq 4000. The datasets are available on the Sequence Read Archive (SRA) of the National Center for Biotechnology (NCBI) under the accession number GSE153534.

(2) Raw FASTQ file processing

Paired-end FASTQ files were uploaded to the Galaxy Human Cell Atlas server, [70] read errors were corrected and cell barcodes demultiplexed using MM3 RNA STARSolo. The reference library for mouse (Ch39/mm39) was used to map the raw aortic single-cell transcriptome reads using the STAR spliced read alignment algorithm.[71] Then, error correction and deduplication of unique molecular identifiers was performed, and the per-cell gene expression was quantified by counting the number of reads per gene.[70]

(3) Clustering Analysis and Integrated Pathway Analysis

Further processing of the data sets was performed in R-Studio using Seurat.[72] Seurat was used for a quality control analysis and single cell transcriptome clustering and visualization in a Uniform Manifold Approximation and Projection Space (UMAP) of the output files obtained by STARSolo.[72] Cells with less than 500 or more than 15000 transcripts were excluded from the analysis. Using the Seurat *FindIntegrationAnchor* function the single-cell data was merged. With the help of Principal Component Analysis for dimensionality reduction, cells were clustered and cluster resolution was set to 0.8 in the FindCluster function in Seurat. We identified marker genes for cluster calling, and then performed differential gene expression analysis.[73] Up- and downregulated genes above a p-value of 0.05 and a log-fold-change between 0.5 and -0.5 were excluded to increase significance. Integrated pathway analysis was performed with ClueGO.[74]

3.2.5 Cell Culture

To investigate the effect of MPO and its derivatives in vitro on smooth muscle cells and the ECM, human aortic smooth muscle cells (HAoSMC) were cultured in Vascular Cell Basal Medium and Vascular Smooth Muscle Cell Growth Kit and ECM was isolated.

For culturing, cells were transferred to cell culture flasks and covered with pre-warmed medium and kept in the incubator at 37°C. Medium was changed every two days, and cell density was checked daily. Passaging was performed by adding 0,5% trypsine twice, which was aspirated after wetting the entire cell layer. After two minutes in the incubator, medium was added to the monolayer, gently resuspended and cell-fluid-mixture was centrifuged in falcons at 1000rpm for three minutes. The medium was gently aspirated and cell pellet was resuspended with fresh medium and then transferred to the incubator in new culture flasks.

When a density of 70% or more was reached, the cells were passaged and transferred to gelantine-coated chamber. For coating, 0.1% gelantine was applied to chamber slides and incubated for two hours, aspirated and slides were allowed to dry for 15 minutes. Chamber slides containing cells were stored in pure VSMC medium without serum for 12 hours to prevent albumin-MPO-interference. ECM isolation was performed in half of the chambers. Therefore, they were washed twice with PBS without calcium or magnesium, before incubation with 0,5% sodium deoxychalate (DOC) for two ten minute periods at room temperature with intermittent rocking. The chamber slides were then washed five times with PBS to remove all cells. All chamber slides, containing either isolated ECM or untreated HAoSMC were divided into different conditions according to the following table (Table 4). Reagents were diluted to the desired concentrations (Table 4), while HOCl was freshly prepared due to its volatile nature. To prevent reaction between MPO and H_2O_2, MPO was applied to the chambers five minutes before H_2O_2. A total of 0.2mL was applied to all chambers. The chamber slides were incubated at 37°C for two hours. Prior to two washes with PBS, isolated ECM chambers were fixed with 4% PFA for ten minutes at room temperature. All chamber slides were stored in PBS at 4°C overnight before immunofluorescence staining for fibronectin, nitrotyrosine, and DAPI to illustrate the effect and accumulation of nitrotyrosine as a downstream product of MPO and its effect on the ECM scaffold.

Control	10µg MPO / 40µM H_2O_2	20µg MPO / 80µM H_2O_2	40µg MPO / 160µM H_2O_2
40µM HOCl	80µM HOCl	10µg MPO	40µM H_2O_2

Table 4 **Treatment conditions for HAoSMC and isolated ECM chamber slides**

3.3 Statistical analysis

All data is presented as ± standard error of the mean (SEM). Brown-Forsythe test was utilized to test for normal distribution and variance equality. Ordinary one-way analysis of variance (ANOVA) with post-hoc Tukey´s test was performed to evaluate differences between groups and normal distribution and equal variance. For comparison of two groups the unpaired t-test was used. A p-value below 0.05 was considered statistically significant. All statistical analyses were performed using GraphPad Prism 8.4.0 (GraphPad Software, San Diego, CA, USA, www.graphpad.com).

4. Results

4.1. Endothelium cell alteration

To evaluate the role of endothelial cells in the disease progression and their alterations in MFS I performed in silico analysis of previously published aortic single cell transcriptomes from WT and MFS mice at the age of 24 months. We identified two endothelial cell clusters expressing the hallmark genes *Pecam 1, Cldn5* and *Ctla2a* (Figure 3B). In EC cluster 1, typical EC-related genes such as endothelial cell-selective adhesion molecule (*Esam)* and tyrosine kinase wit immunoglobulin like and EGF like domains 1 (*Tie1)* were predominantly expressed. *Esam* encodes for a cell adhesion molecule of vascular endothelial cells responsible for angiogenesis, permeability and leukocyte transmigration.[75,76,77] *Tie1* is an angiopoetin receptor that regulates angiogenesis and EC survival, triggered by inflammatory processes.[78,79] EC cluster 2 was smaller and characterized by *Nts2*, *Ccl21a*, *Fabp4,* and *Lyve-1* expression (Figure 3B). Lymphatic vessel endothelial hyaluronic acid receptor 1 *(Lyve1)* is a hyaluronan receptor mainly expressed on lymphatic endothelial cells that also secrete CC-chemokine ligand 21 (*CCL21)*, which is responsible for dendritic cell migration and is upregulated by inflammation.[80,81] These characteristic genes suggest that EC cluster 2 contains lymphatic ECs. Differential gene expression analysis of the two EC clusters in MFS mice revealed 242 differentially regulated genes in EC cluster 1 and 196 in EC cluster 2. Both EC populations shared 55 upregulated genes indicative of endothelial to mesenchymal transition including *Acta2, Tagln, Myl9* and *Itga8,* and several collagen-encoding genes. The 43 common downregulated genes in MFS include EC marker genes such as *Pecam1, Cldn5,* and *Cdh5*. Cell migration and inflammation related genes were expressed in both EC clusters. EC cluster 1 showed *Cxcl2, Cxcl12* and *Vcan* expression, EC cluster 2 expressed *Ccll4, Cxcl1* and *Ncam1* (Figure 3C, D). Gene term analysis further revealed enrichment for pathways involved in inflammation (granulocyte chemotaxis and endothelial cell migration) and extracellular matrix remodeling regarding TGF-ß-receptor signaling pathways, wound healing, collagen fibril and ECM organization and collagen metabolism. Pathways related to endothelial cell development and differentiation (*endothelium development, regulation of endothelial cell proliferation, regulation of endothelial cell migration*) and angiogenesis (*vasculogenesis, regulation of angiogenesis angiogenesis, sprouting angiogenesis*) are downregulated in both EC clusters (Figure 3E, F). The NO biosynthesis pathway is inactivated in MFS ECs, resulting in impaired vascular function.[32]

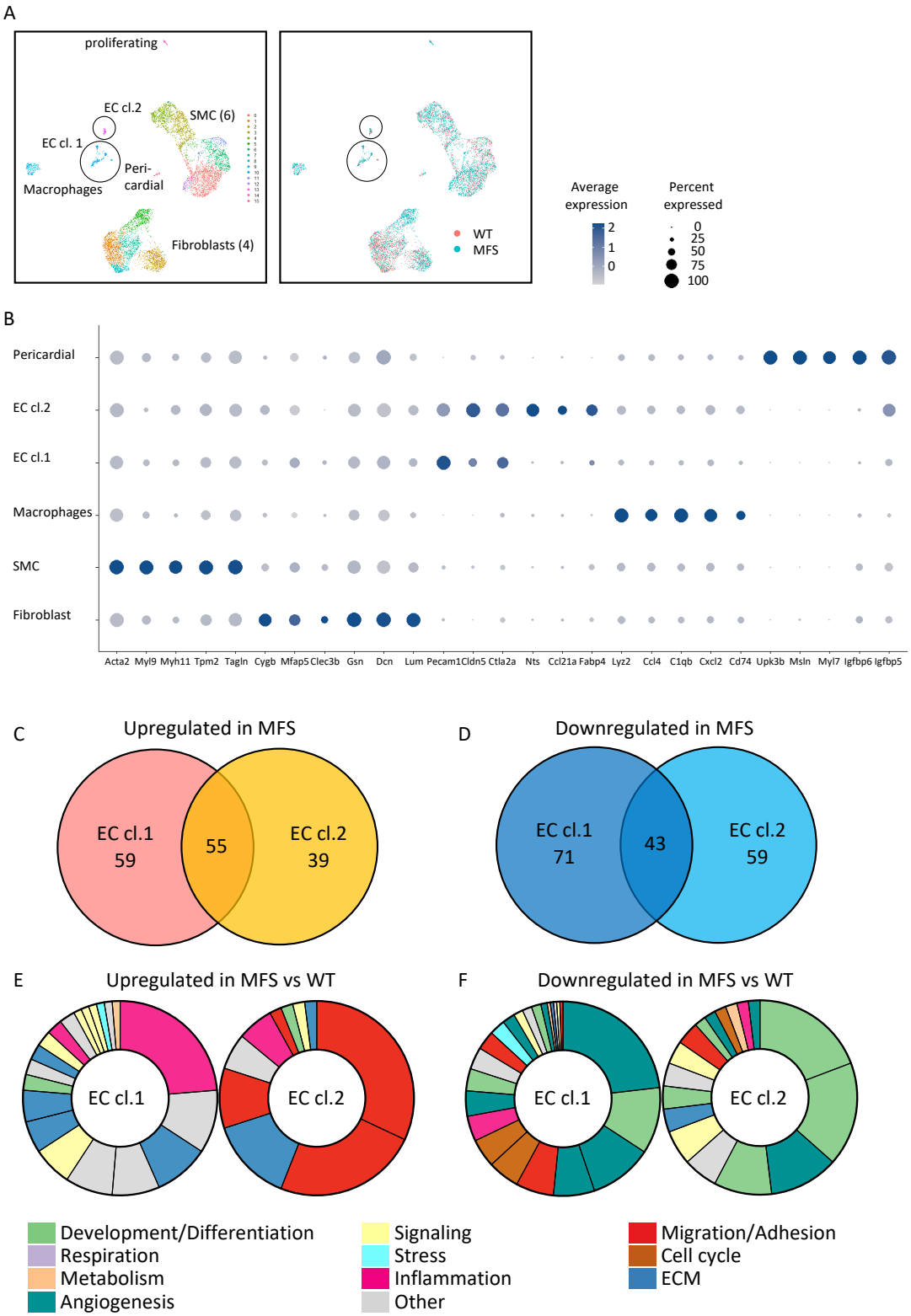

Figure 3 In silico analysis

(A, B) In silico analysis of aortic single-cell transcriptomes obtained from WT and MFS mice.[69] Two EC clusters were identified and marker genes are reported. Venn diagrams demonstrate number of (C) upregulated and (D) downregulated genes in the EC clusters in MFS compared to WT mice. Gene pathway analysis of (E) upregulated and (F) downregulated genes in EC clusters in MFS compared to WT.

4.2. Immune cell infiltration

Leukocytes are attracted by chemokines and rely on adhesion molecules such as integrins for rolling, adhesion and transmigration.[82] ECs increase expression if ICAM-1 due to the influence of inflammation, cytokines, and ROS pathways. This phenotypic change to ECs plays an important role in the leukocyte migration cascade.[83] vWF-positive ECs in the aortic root from MFS mice showed higher levels of endothelium bound ICAM-1 than MFSxMPO$^{-/-}$ or control groups, suggesting that ECs are more activated and that more transmigration occurs in MFS than in WT and MFSxMPO$^{-/-}$ (Figure 5).

Intravital microscopy of the cremaster muscle arteries was used to observe inflammatory endothelial activation in vivo and determine its pathophysiological relevance. Therefore, the leukocyte rolling time and distance, speed, and adhesion time was quantified. While the time and distance of leukocyte rolling was significantly higher in MFS compared to MFSxMPO$^{-/-}$, the speed was lower, indicating an increased affinity to the vessel wall through higher expression of integrins and adhesion molecules.[84] The adhesion time of leukocytes to the endothelium was drastically reduced in MFSxMPO$^{-/-}$ mice, as was the total number of leukocytes observed (Figure 6). The reduced leukocyte diapedesis and lower activation status of aortic EC in MFSxMPO$^{-/-}$ compared to MFS suggests that the inflammatory response in MFS is attenuated due to MPO deficiency.

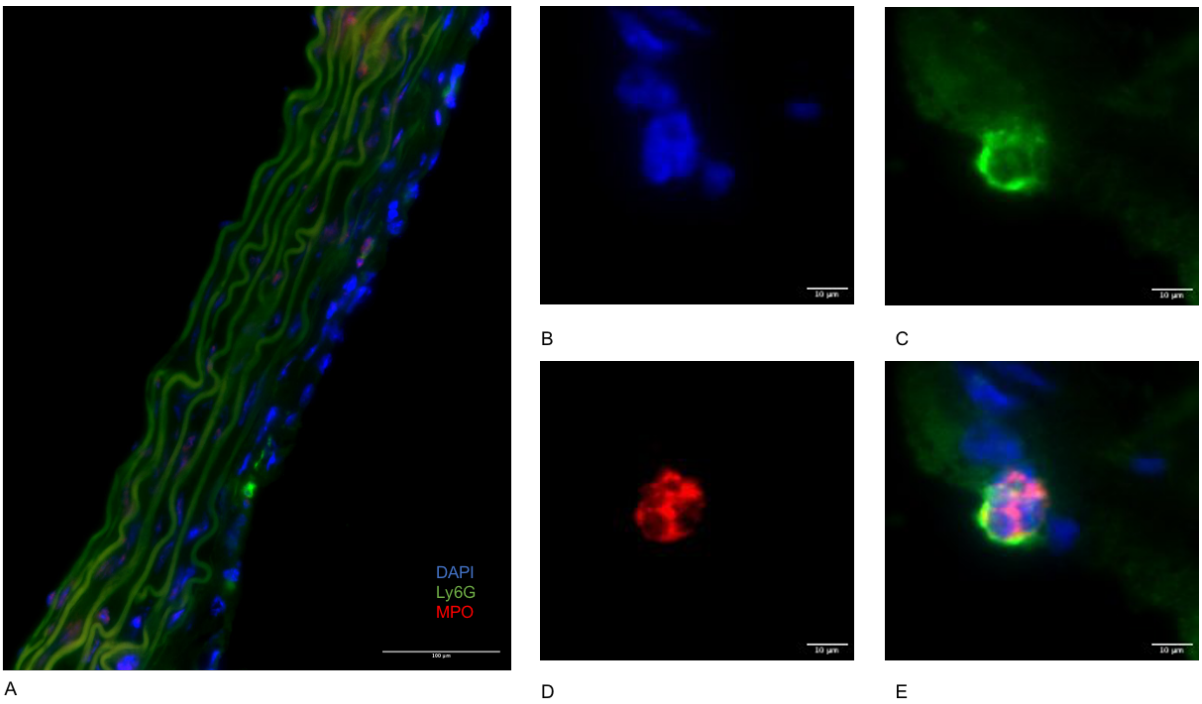

Figure 4 Representative IF image of a leukocyte in the ascending aorta of an MFS mouse

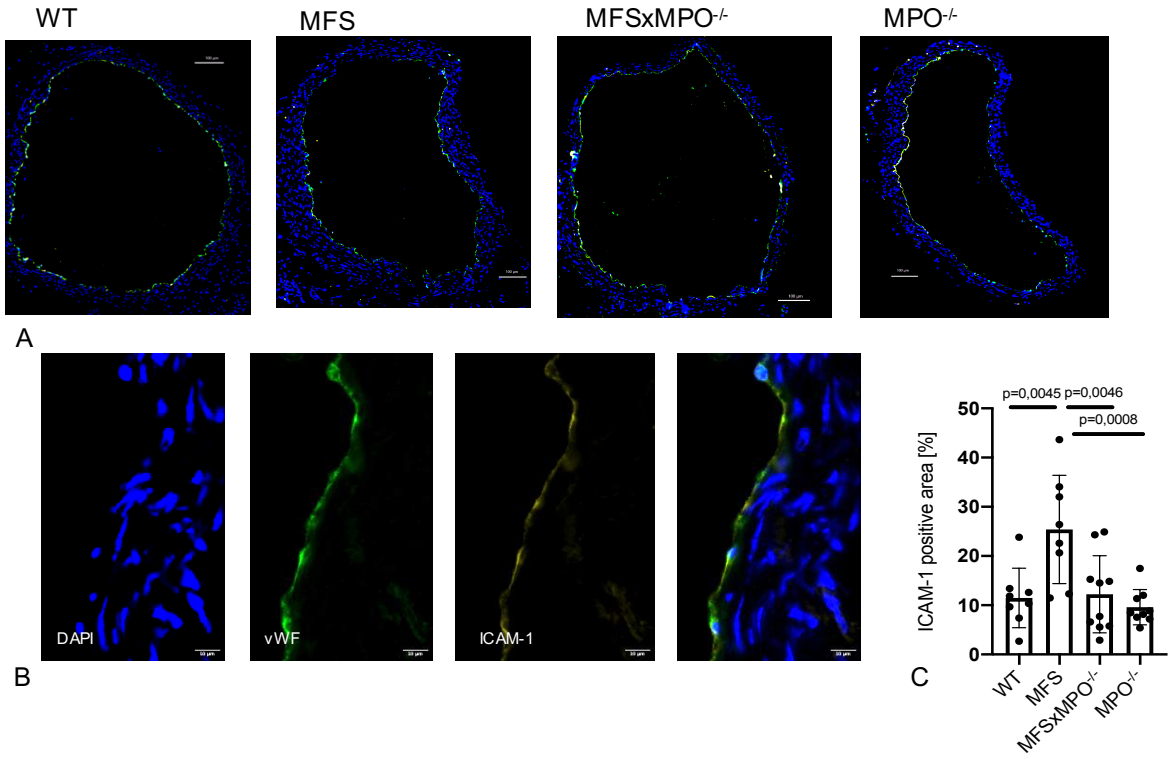

Figure 5 EC activation is reduced in MPO-deficient MFS mice

(A) Representative immunofluorescence images of ascending aortic cross-sections co-stained for vWF (green) and ICAM-1 (yellow). The frequency of double positive cells was quantified (N=8-10/group). (B) Magnification of MFS aortic cross-section (C) Quantification of ICAM-1 signal relative to vWF positive area in percentage (%). Data is presented as mean ± SEM. Statistical significance was determined by ordinary one-way ANOVA followed by Tukey's multiple comparison test.

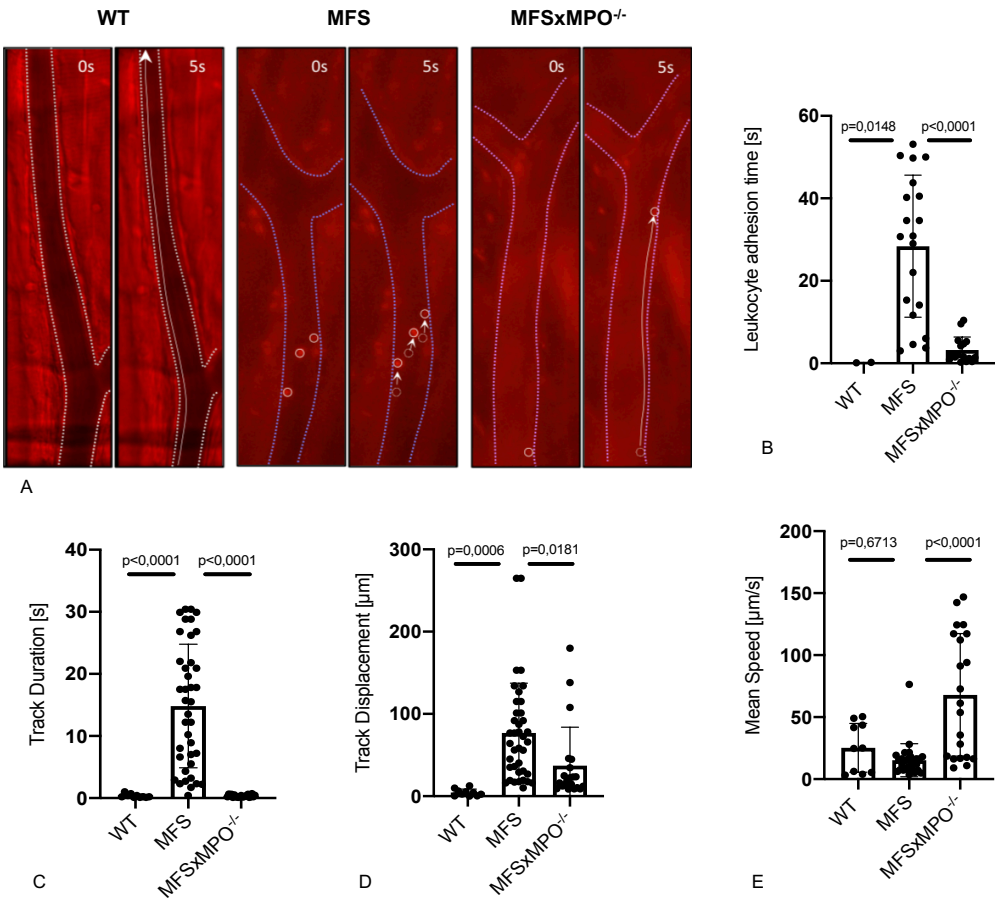

Figure 6 Vascular Inflammation is reduced in MPO-deficient MFS mice

(A) Representative images of intravital microscopy of the cremaster muscle with indicated leukocyte rolling distance within 5 seconds. Quantification of (B) adhesion time, (C) rolling time, (D) rolling distance, and (E) rolling speed. Data is presented as mean ± SEM. Statistical significance was determined by ordinary one-way ANOVA followed by Tukey's multiple comparison test.

4.3. MAPK/ERK signaling pathway alteration

An Immunoblot analysis performed for ERK1/2 and phosphorylated ERK1/2 shows downregulation in MFSxMPO$^{-/-}$ as compared to MFS. As ERK is a mediator of the non-canonical TGF-ß signaling pathway, regulating cell proliferation and survival, and is known to drive TAA formation in MFS,[23,85] this indicates that in MPO deficient MFS mice, pathways ultimately leading to TAA formation are attenuated. As shown by Mu et al. nitrotyrosine leads to phosphorylation of ERK2 and thereby to an activation of the MAPK pathway, [86] explaining why, in the absence of MPO, there is less activation of ERK.

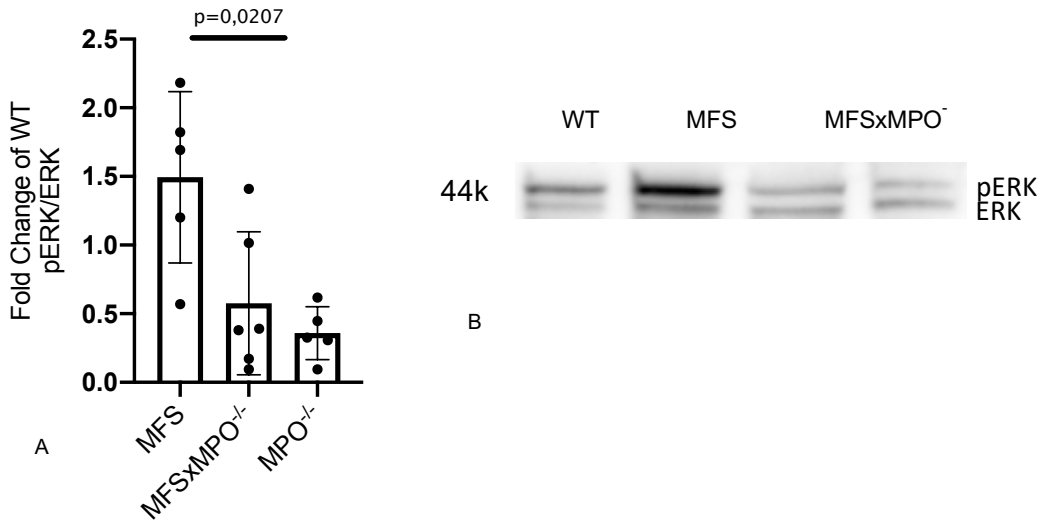

Figure 7 Western Blot analysis of ERK1/2 and pERK1/2

(A) Immunoblot analysis of phosphorylated ERK1/2 normalized to ERK1/2 (n=6 per group) was normalized to the fold change of the wild-type mouse group, (B) representative image of an Immunoblot band at 44 kDa with phosphorylated ERK as the top band and ERK1/2 as the bottom band. Data is presented as mean ± SEM. Statistical significance was determined by ordinary one-way ANOVA followed by Tukey's multiple comparison test.

4.4. Nitrosation in VSMC and ECM

Treating HAoSMCs and their produced and isolated ECM with MPO and its derivatives, illustrates the damage of MPO and ROS on the vasculature.

Myeloperoxidase produces 3-nitrotyrosine using H_2O_2 and nitrite as substrates.[87] Nitrotyrosine serves as a marker of oxidative stress and inflammation and drives AoSMC migration, ROS production and phosphorylation of ERK2.[86] After treatment of cells and ECM with MPO, H_2O_2, or HOCl, nitrotyrosine was produced and infiltrated the VSMCs and accumulated around the nucleus (Figure 8C,D). Further it can be seen that fibronectin, part of the ECM scaffold, is destructed after MPO and HOCl treatment. Fibronectin is essential for fibrillin organization, as demonstrated in in-vitro experiments with dermal fibroblasts.[88] As shown by Baldus et al, MPO transcytoses endothelium and leads to posttranslational modification of fibronectin.[44]

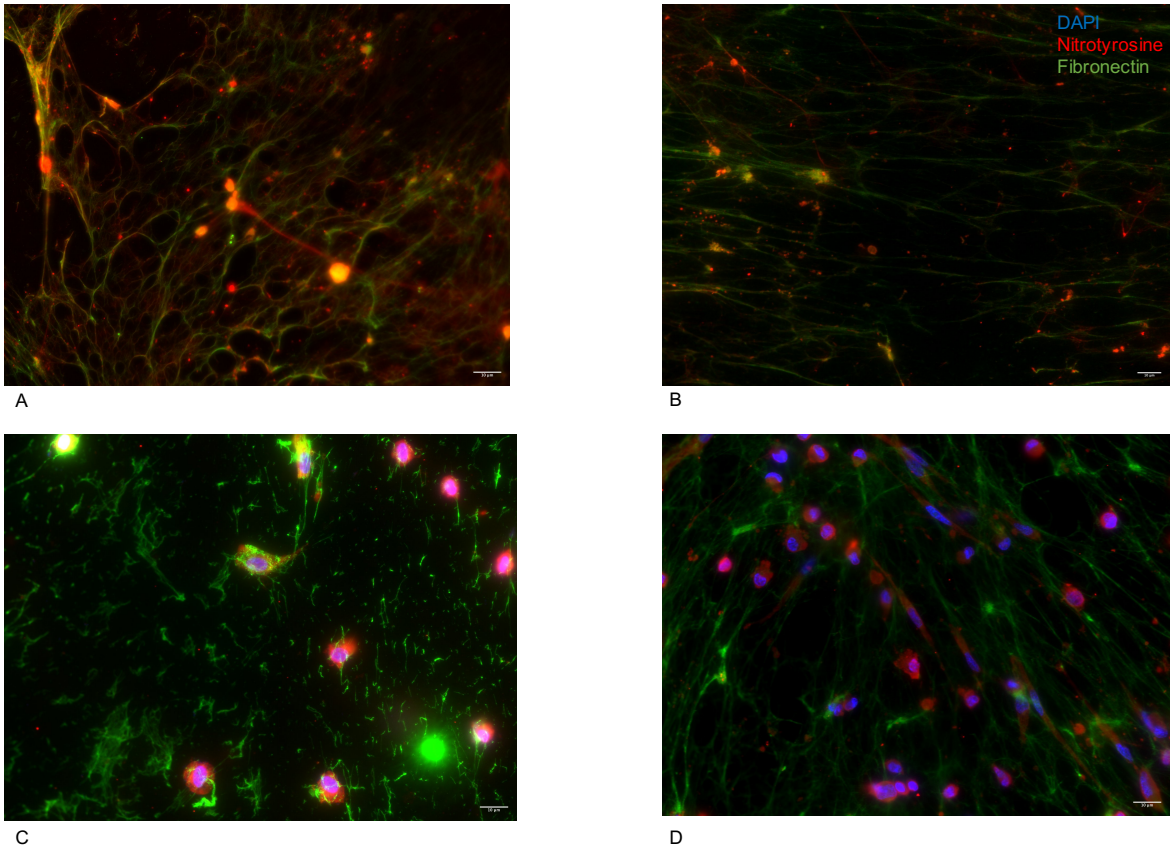

Figure 8 Treatment of hAoSMC and isolated ECM with MPO and its derivatives for 2 hours

(A) Isolated ECM treated with 10µg MPO and 40 µM H_2O_2, (B) Isolated ECM treated with 80µM HOCl, (C) hAoSMC treated with 10µg MPO and 40 µM H_2O_2, (D) hAoSMC treated with 80µM HOCl

5. Discussion

In conclusion, it is revealed that MPO is involved in inflammatory processes in MFS, that EC alteration and activation occur in MFS, and that activation and inflammation are attenuated by MPO depletion in a murine mouse model of MFS. In MFS, ascending aortic ECs show increased expression of adhesion molecules such as ICAM-1 compared to MFSxMPO$^{-/-}$ and WT. Furthermore, the scRNAseq of MFS and WT ECs revealed EC differentiation into two subclusters. Inflammation, ECM remodeling, wound healing, and collagen metabolism pathways are enriched, whereas EC development, differentiation, and angiogenesis pathways are downregulated in MFS compared to WT. Activation of ECs leads to increased leukocyte diapedesis as demonstrated by intravital microscopy. Cell culture experiments with HAoSMCs and their ECM demonstrated nitrosation of VSMCs and destruction of the ECM construct. Western blot analysis shows a trend towards downregulation of a commonly known pathway involved in MFS pathogenesis, the non-canonical TGF-β signaling via ERK, in MPO deficient MFS mice.

Increased levels of neutrophil-derived MPO are associated with a higher risk of cardiovascular disease.[89] MPO serum levels have been shown to correlate with endothelial dysfunction.[90] This work demonstrates that in MFS, ECs are activated and prone to enhance inflammatory responses within the aortic wall through the increased expression of ICAM-1 on the EC surface. This leads to increased leukocyte infiltration, all of which are attenuated by MPO depletion in MFS. Inflammation has been shown to lead to upregulation of ICAM-1 expression on ECs.[81] More ICAM-1 expression leads to more leukocyte diapedesis and therefore inflammation in the aortic wall.[91] Increased leukocyte transmigration results in more MPO release into the aortic wall, accelerating EC dysfunction and vascular remodeling through oxidative stress, creating a vicious cycle. MPO and its products impair endothelial NO bioactivity,[92] and thereby reduce endothelium dependent relaxation,[93] correlating with the scRNAseq finding showing a downregulation of the NO biosynthesis pathway in EC cluster 1 in MFS. Pharmacologic inhibition of MPO results in improved endothelial function and decreased enzymatic activity in arterial tissue.[94] MPO depletion, both pharmacologic and genetic, leads to significantly reduced inflammatory responses, attenuation of aortic root aneurysm growth, MMP activation, and elastic fiber fragmentation in MFS mice.[95]

Up until now, excessive TGF-β signaling was believed to be the driving factor for MFS related TAA formation.[23] The only therapeutic options include Losartan and β-blockers, which prevented aortic dilation in a mouse model.[24] Subsequent clinical trials could validate attenuation of aortic root dilation by Losartan for human MFS patients.[96] Clinical endpoints like dissection, aortic surgery or cardiovascular death did not significantly differ from patients treated with beta blockers alone.[96,97] Although there is increasing evidence for the involvement of inflammatory processes in the progression of MFS, detailed knowledge of pathways, causes and consequences is scarce, and no new therapeutic targets have been clinically tested.[36,98,99,100]

Seeing that MPO inhibition in mice proves to be a potent treatment to slow the rate of TAA growth, it has to be further proven for humans.[95] Plasma MPO levels have been found to correlate with several cardiovascular diseases.[101] Measurements of plasma from MFS patients showed significantly elevated MPO levels, as well as MPO deposition in aortic root sections.[95] This suggests that humans suffering from MFS can be detected through MPO measurement and might benefit from pharmacologic MPO inhibition.

5.1. Limitations and strengths

The differences in age of the mice used for IF, intravital microscopy and immunoblots compared to the scRNAseq mice can be viewed as a limitation of this work. Unfortunately, the mice used for scRNAseq were both female and male and were analyzed at 4 and 24 weeks of age, while all the other experiments were performed on 12-week-old male mice only. It can be argued that the 24-week analysis may reflect end stage disease outcomes rather than the driving mechanisms for TAA development. Another limitation is the absence of the MFSxMPO$^{-/-}$ group in the in-silico analysis leaving open the question whether MPO deficiency, and more importantly, pharmacological MPO inhibition could reverse the observed effects as for example EC alteration. Still the results obtained by scRNAseq prove that relevant pathway and gene expression alterations happen in MFS ECs at both time points assessed. As correlating results were obtained using immunofluorescence (IF) and intravital microscopy, despite the age difference, it can be concluded that inflammation is a driving factor at different stages of the disease.

Intravital microscopy was successfully performed on the cremaster artery, which is widely regarded the most suitable option for such imaging studies due to its practicality. However, intravital imaging of the ascending aorta has not yet been achieved due to experimental limitations, including the technical and anatomical challenges associated with imaging this region in vivo. Despite the limitations previously mentioned, which have precluded detailed examination of the ascending aorta, studies have demonstrated that visceral arteries are also affected by MFS.[102] This finding serves to reinforce the hypothesis that the inflammatory processes in this condition are of systemic nature. The results of the experiment show a significant difference in leukocyte rolling, number and adhesion. The observed differences in small peripheral vessels and their correlation with the elevated expression levels of ICAM-1 in the aortic arch, along with the altered activities of migration and inflammatory pathways in aortic EC, have been validated by IF and scRNAseq. These findings suggest the presence of heightened inflammatory responses in these regions.

It cannot be excluded that MPO affects MFS-related TAA formation by additional mechanisms. Clinical endpoints such as aortic rupture or dissection were not examined because the mouse model used does not develop these end stage disease pathologies. Thus, findings in the murine MFS model cannot be applied unconditionally to human MFS patients.

5.2. Implications for further research

All of the above results indicate that MPO plays an important role in the pathogenesis of aortic aneurysm formation in MFS. A direct measurement of MPO activity could further substantiate this. PMNs are the main carriers of MPO and therefore an interesting target to look at more closely to see if they differ in activation or function in MFS. MFS mice could be treated with pharmacological MPO inhibitors to elucidate the therapeutic efficacy and possible side effects of a therapeutic intervention. Consecutively, as pharmacological oral MPO inhibitors have been proven in efficacy and safety in humans, further clinical trials of MPO inhibitors in MFS patients would be feasible.[103] To investigate the role of endothelial activation through ICAM-1 further and to distinguish whether the enhanced ICAM-1 activation is an effect or a driving factor in MFS pathogenesis, mice could be treated with pharmacological ICAM-1 inhibitors. Alternatively, a mouse line with a genetic conditional ICAM-1 knockout could be bred and investigated.

6. Literature

1 Cardiovascular diseases (CVDs). https://www.who.int/news-room/fact-sheets/detail/cardiovascular-diseases-(cvds) (accessed Aug 31, 2021).

2 GA R, GA M, CO J, *et al.* Global Burden of Cardiovascular Diseases and Risk Factors, 1990-2019: Update From the GBD 2019 Study. *J Am Coll Cardiol* 2020; **76**: 2982–3021.

3 Gaidai O, Cao Y, Loginov S. Global Cardiovascular Diseases Death Rate Prediction. *Curr Probl Cardiol* 2023; **48**: 101622.

4 Lindsay ME, Dietz HC. Lessons on the pathogenesis of aneurysm from heritable conditions. *Nat 2011 4737347* 2011; **473**: 308–16.

5 Goldfinger JZ, Halperin JL, Marin ML, Stewart AS, Eagle KA, Fuster V. Thoracic aortic aneurysm and dissection. *J Am Coll Cardiol* 2014; **64**: 1725–39.

6 Booher AM, Eagle KA. Diagnosis and management issues in thoracic aortic aneurysm. *Am Heart J* 2011; **162**: 38-46.e1.

7 Chen SW, Kuo CF, Huang YT, *et al.* Association of Family History With Incidence and Outcomes of Aortic Dissection. *J Am Coll Cardiol* 2020; **76**: 1181–92.

8 Rodrigues Bento J, Meester J, Luyckx I, Peeters S, Verstraeten A, Loeys B. The Genetics and Typical Traits of Thoracic Aortic Aneurysm and Dissection. *Annu Rev Genomics Hum Genet* 2022; **23**: 223–53.

9 Surman TL, Abrahams JM, Manavis J, *et al.* Histological regional analysis of the aortic root and thoracic ascending aorta: a complete analysis of aneurysms from root to arch. *J Cardiothorac Surg* 2021; **16**: 1–10.

10 Skotsimara G, Antonopoulos A, Oikonomou E, Papastamos C, Siasos G, Tousoulis D. Aortic Wall Inflammation in the Pathogenesis, Diagnosis and Treatment of Aortic Aneurysms. *Inflammation* 2022; **45**: 965—976.

11 Jauhiainen S, Kiema M, Hedman M, Laakkonen JP. Large Vessel Cell Heterogeneity and Plasticity: Focus in Aortic Aneurysms. *Arterioscler Thromb Vasc Biol* 2022; **42**: 811–8.

12 Verstraeten A, Fedoryshchenko I, Loeys B. The emerging role of endothelial cells in the pathogenesis of thoracic aortic aneurysm and dissection. *Eur Heart J* 2023; **00**: 1–3.

13 Petsophonsakul P, Furmanik M, Forsythe R, *et al.* Role of Vascular Smooth Muscle Cell Phenotypic Switching and Calcification in Aortic Aneurysm Formation. *Arterioscler Thromb Vasc Biol* 2019; **39**: 1351–68.

14 Salik I, Rawla P. Marfan syndrome. *StatPearls Publ* 2020; **46**: 92–8.

15 Judge DP, Dietz HC. Marfan's syndrome. *Lancet* 2005; **366**: 1965–76.

16 Murdoch JL, Walker BA, Halpern BL, Kuzma JW, McKusick VA. Life Expectancy and Causes of Death in the Marfan Syndrome. *N Engl J Med* 1972; **286**: 804–8.

17 Sakai LY, Keene DR, Glanville RW, Bachinger HP. Purification and partial

characterization of fibrillin, a cysteine-rich structural component of connective tissue microfibrils. *J Biol Chem* 1991; **266**: 14763–70.

18 Sakai LY, Keene DR, Engvall E. Fibrillin, a new 350-kD glycoprotein, is a component of extracellular microfibrils. *J Cell Biol* 1986; **103**: 2499–509.

19 Ramirez F, Sakai LY. Biogenesis and function of fibrillin assemblies. *Cell Tissue Res* 2010; **339**: 71–82.

20 Asano K, Cantalupo A, Sedes L, Ramirez F. Pathophysiology and Therapeutics of Thoracic Aortic Aneurysm in Marfan Syndrome. *Biomolecules* 2022; **12**. DOI:10.3390/biom12010128.

21 Bunton TE, Biery NJ, Myers L, Gayraud B, Ramirez F, Dietz HC. Phenotypic Alteration of Vascular Smooth Muscle Cells Precedes Elastolysis in a Mouse Model of Marfan Syndrome. *Circ Res* 2001; **88**: 37–43.

22 Pedroza AJ, Tashima Y, Shad R, *et al.* Single-Cell Transcriptomic Profiling of Vascular Smooth Muscle Cell Phenotype Modulation in Marfan Syndrome Aortic Aneurysm. *Arterioscler Thromb Vasc Biol* 2020; : 2195–211.

23 Holm TM, Habashi JP, Doyle JJ, *et al.* Noncanonical TGFβ Signaling Contributes to Aortic Aneurysm Progression in Marfan Syndrome Mice. *Science (80-)* 2011; **332**: 358–61.

24 Habashi JP, Judge DP, Holm TM, *et al.* Losartan, an AT1 Antagonist, Prevents Aortic Aneurysm in a Mouse Model of Marfan Syndrome. *Science (80-)* 2006; **312**: 117–21.

25 Pedroza AJ, Koyano T, Trojan J, *et al.* Divergent effects of canonical and non-canonical TGF-β signalling on mixed contractile-synthetic smooth muscle cell phenotype in human Marfan syndrome aortic root aneurysms. *J Cell Mol Med* 2020; **24**: 2369–83.

26 Holm TM, Habashi JP, Doyle JJ, *et al.* Noncanonical TGF\&\#x3b2; Signaling Contributes to Aortic Aneurysm Progression in Marfan Syndrome Mice. *Science (80-)* 2011; **332**: 358–61.

27 Gomez D, Al Haj Zen A, Borges LF, *et al.* Syndromic and non-syndromic aneurysms of the human ascending aorta share activation of the Smad2 pathway. *J Pathol* 2009; **218**: 131–42.

28 Tehrani AY, Cui JZ, Bucky Jones T, *et al.* Characterization of doxycycline-mediated inhibition of Marfan syndrome-associated aortic dilation by multiphoton microscopy. *Sci Rep* 2020; **10**: 7154.

29 Chung AWY, Yang HHC, Radomski MW, van Breemen C. Long-Term Doxycycline Is More Effective Than Atenolol to Prevent Thoracic Aortic Aneurysm in Marfan Syndrome Through the Inhibition of Matrix Metalloproteinase-2 and -9. *Circ Res* 2008; **102**: e73–85.

30 de la Fuente-Alonso A, Toral M, Alfayate A, *et al.* Aortic disease in Marfan syndrome is

caused by overactivation of sGC-PRKG signaling by NO. *Nat Commun* 2021; **12**: 2628.

31 Portelli SS, Hambly BD, Jeremy RW, Robertson EN. Oxidative stress in genetically triggered thoracic aortic aneurysm: role in pathogenesis and therapeutic opportunities. *Redox Rep* 2021; **26**: 45–52.

32 Chung AWY, Au Yeung K, Cortes SF, *et al.* Endothelial dysfunction and compromised eNOS/Akt signaling in the thoracic aorta during the progression of Marfan syndrome. *Br J Pharmacol* 2007; **150**: 1075–83.

33 Emrich F, Penov K, Arakawa M, *et al.* Anatomically specific reactive oxygen species production participates in Marfan syndrome aneurysm formation. *J Cell Mol Med* 2019; **23**: 7000–9.

34 Li C, Meng X, Wang L, Dai X. Mechanism of action of non-coding RNAs and traditional Chinese medicine in myocardial fibrosis: Focus on the TGF-β/Smad signaling pathway. *Front Pharmacol* 2023; **14**. DOI:10.3389/fphar.2023.1092148.

35 Radonic T, de Witte P, Groenink M, et al. Inflammation aggravates disease severity in Marfan syndrome patients. PLoS One. 2012;7(3):e32963. doi:10.1371/journal.pone.0032963. .

36 Radonic T, de Witte P, Groenink M, *et al.* Inflammation aggravates disease severity in marfan syndrome patients. *PLoS One* 2012; **7**: 1–9.

37 He R, Guo D-C, Sun W, *et al.* Characterization of the inflammatory cells in ascending thoracic aortic aneurysms in patients with Marfan syndrome, familial thoracic aortic aneurysms, and sporadic aneurysms. *J Thorac Cardiovasc Surg* 2008; **136**: 922-929.e1.

38 Guo G, Booms P, Halushka M, *et al.* Induction of Macrophage Chemotaxis by Aortic Extracts of the mgR Marfan Mouse Model and a GxxPG-Containing Fibrillin-1 Fragment. *Circulation* 2006; **114**: 1855–62.

39 Guo G, Gehle P, Doelken S, *et al.* Induction of Macrophage Chemotaxis by Aortic Extracts from Patients with Marfan Syndrome Is Related to Elastin Binding Protein. *PLoS One* 2011; **6**: 1–7.

40 van der Veen BS, de Winther MPJ, Heeringa P. Myeloperoxidase: Molecular Mechanisms of Action and Their Relevance to Human Health and Disease. *Antioxid Redox Signal* 2009; **11**: 2899–937.

41 Lau D, Baldus S. Myeloperoxidase and its contributory role in inflammatory vascular disease. *Pharmacol Ther* 2006; **111**: 16–26.

42 Klinke A, Nussbaum C, Kubala L, *et al.* Myeloperoxidase attracts neutrophils by physical forces. *Blood* 2011; **117**: 1350–8.

43 Cai H, Chuang CY, Hawkins CL, Davies MJ. Binding of myeloperoxidase to the extracellular matrix of smooth muscle cells and subsequent matrix modification. *Sci Rep*

2020; **10**: 666.

44 Baldus S, Eiserich JP, Mani A, *et al.* Endothelial transcytosis of myeloperoxidase confers specificity to vascular ECM proteins as targets of tyrosine nitration. *J Clin Invest* 2001; **108**: 1759–70.

45 Heinecke JW. Mechanisms of oxidative damage by myeloperoxidase in atherosclerosis and other inflammatory disorders. *J Lab Clin Med* 1999; **133**: 321–5.

46 Anatoliotakis N, Deftereos S, Bouras G, *et al.* Myeloperoxidase: Expressing Inflammation and Oxidative Stress in Cardiovascular Disease. *Curr Top Med Chem* 2013; **13**: 115–38.

47 Thai T, Zhong F, Dang L, *et al.* Endothelial-transcytosed myeloperoxidase activates endothelial nitric oxide synthase via a phospholipase C-dependent calcium signaling pathway. *Free Radic Biol Med* 2021; **166**: 255–64.

48 Mehrkens D, Dohr JK, Mollenhauer M, *et al.* P4551Myeloperoxidase activity aggravates aortic wall remodeling and participates in aneurysm development in Marfan Syndrome. *Eur Heart J* 2018; **39**. DOI:10.1093/eurheartj/ehy563.P4551.

49 Nussbaum C, Klinke A, Adam M, Baldus S, Sperandio M. Myeloperoxidase: A Leukocyte-Derived Protagonist of Inflammation and Cardiovascular Disease. *Antioxidants \& Redox Signal* 2013; **18**: 692–713.

50 Scharnagl H, Kleber ME, Genser B, *et al.* Association of myeloperoxidase with total and cardiovascular mortality in individuals undergoing coronary angiography—The LURIC study. *Int J Cardiol* 2014; **174**: 96–105.

51 Kim HW, Blomkalns AL, Ogbi M, *et al.* Role of myeloperoxidase in abdominal aortic aneurysm formation: mitigation by taurine. *Am J Physiol Circ Physiol* 2017; **313**: H1168–79.

52 Ollikainen E, Tulamo R, Lehti S, *et al.* Myeloperoxidase Associates With Degenerative Remodeling and Rupture of the Saccular Intracranial Aneurysm Wall. *J Neuropathol Exp Neurol* 2018; **77**: 461–8.

53 Lin W, Chen H, Chen X, Guo C. The Roles of Neutrophil-Derived Myeloperoxidase (MPO) in Diseases: The New Progress. *Antioxidants* 2024; **13**: 132.

54 Pahwa R, Modi P, Jialal I. Myeloperoxidase Deficiency. *StatPearls Publ Treasure Isl* 2020.

55 Keane MG, Pyeritz RE. Medical Management of Marfan Syndrome. *Circulation* 2008; **117**: 2802–13.

56 Lacro R V, Dietz HC, Sleeper LA, *et al.* Atenolol versus Losartan in Children and Young Adults with Marfan's Syndrome. *N Engl J Med* 2014; **371**: 2061–71.

57 Pinard A, Jones GT, Milewicz DM. Genetics of Thoracic and Abdominal Aortic Diseases. *Circ Res* 2019; **124**: 588–606.

58 Carman C V, Martinelli R. T Lymphocyte–Endothelial Interactions: Emerging Understanding of Trafficking and Antigen-Specific Immunity. *Front Immunol* 2015; **6**. DOI:10.3389/fimmu.2015.00603.

59 van de Pol V, Kurakula K, DeRuiter MC, Goumans M-J. Thoracic Aortic Aneurysm Development in Patients with Bicuspid Aortic Valve: What Is the Role of Endothelial Cells? *Front Physiol* 2017; **8**. DOI:10.3389/fphys.2017.00938.

60 Amersfoort J, Eelen G, Carmeliet P. Immunomodulation by endothelial cells - partnering up with the immune system? *Nat Rev Immunol* 2022; **22**: 576–88.

61 Middleton J, Patterson AM, Gardner L, Schmutz C, Ashton BA. Leukocyte extravasation: chemokine transport and presentation by the endothelium. *Blood* 2002; **100**: 3853–60.

62 Chistiakov DA, Orekhov AN, Bobryshev Y V. Effects of shear stress on endothelial cells: go with the flow. *Acta Physiol* 2017; **219**: 382–408.

63 Yang X, Xu C, Yao F, *et al.* Targeting endothelial tight junctions to predict and protect thoracic aortic aneurysm and dissection. *Eur Heart J* 2023. DOI:10.1093/eurheartj/ehac823.

64 Card CM, Yu SS, Swartz MA. Emerging roles of lymphatic endothelium in regulating adaptive immunity. *J Clin Invest* 2014; **124**: 943–52.

65 Jalkanen S, Salmi M. Lymphatic endothelial cells of the lymph node. *Nat Rev Immunol* 2020; **20**: 566–78.

66 Müller AM, Hermanns MI, Skrzynski C, Nesslinger M, Müller K-M, Kirkpatrick CJ. Expression of the Endothelial Markers PECAM-1, vWf, and CD34 in Vivo and in Vitro. *Exp Mol Pathol* 2002; **72**: 221–9.

67 Schindelin J, Arganda-Carreras I, Frise E, *et al.* Fiji: an open-source platform for biological-image analysis. *Nat Methods 2012 97* 2012; **9**: 676–82.

68 Tinevez JY, Perry N, Schindelin J, *et al.* TrackMate: An open and extensible platform for single-particle tracking. *Methods* 2017; **115**: 80–90.

69 Pedroza AJ, Tashima Y, Shad R, *et al.* Single-Cell Transcriptomic Profiling of Vascular Smooth Muscle Cell Phenotype Modulation in Marfan Syndrome Aortic Aneurysm. *Arterioscler Thromb Vasc Biol* 2020; **40**: 2195–211.

70 Moreno P, Huang N, Manning JR, *et al.* User-friendly, scalable tools and workflows for single-cell analysis. *bioRxiv* 2020. DOI:10.1101/2020.04.08.032698.

71 Dobin A, Davis CA, Schlesinger F, *et al.* STAR: ultrafast universal RNA-seq aligner. *Bioinformatics* 2013; **29**: 15–21.

72 Hao Y, Hao S, Andersen-Nissen E, *et al.* Integrated analysis of multimodal single-cell data. *Cell* 2021; **184**: 3573-3587.e29.

73 Tekman M, Batut B, Ostrovsky A, *et al.* A single-cell RNA-sequencing training and

analysis suite using the Galaxy framework. *Gigascience* 2020; **9**. DOI:10.1093/gigascience/giaa102.

74 Bindea G, Mlecnik B, Hackl H, *et al.* ClueGO: a Cytoscape plug-in to decipher functionally grouped gene ontology and pathway annotation networks. *Bioinformatics* 2009; **25**: 1091–3.

75 Hirata K, Ishida T, Penta K, *et al.* Cloning of an Immunoglobulin Family Adhesion Molecule Selectively Expressed by Endothelial Cells*. *J Biol Chem* 2001; **276**: 16223–31.

76 Ishida T, Kundu RK, Yang E, Hirata K, Ho Y-D, Quertermous T. Targeted Disruption of Endothelial Cell-selective Adhesion Molecule Inhibits Angiogenic Processes in Vitro and in Vivo *. *J Biol Chem* 2003; **278**: 34598–604.

77 Wegmann F, Petri B, Khandoga AG, *et al.* ESAM supports neutrophil extravasation, activation of Rho, and VEGF-induced vascular permeability . *J Exp Med* 2006; **203**: 1671–7.

78 Yabkowitz R, Meyer S, Black T, Elliott G, Merewether LA, Yamane HK. Inflammatory Cytokines and Vascular Endothelial Growth Factor Stimulate the Release of Soluble Tie Receptor From Human Endothelial Cells Via Metalloprotease Activation. *Blood* 1999; **93**: 1969–79.

79 Sato TN, Qin Y, Kozak CA, Audus KL. Tie-1 and tie-2 define another class of putative receptor tyrosine kinase genes expressed in early embryonic vascular system. *Proc Natl Acad Sci* 1993; **90**: 9355–8.

80 Prevo R, Banerji S, Ferguson DJP, Clasper S, Jackson DG. Mouse LYVE-1 Is an Endocytic Receptor for Hyaluronan in Lymphatic Endothelium*. *J Biol Chem* 2001; **276**: 19420–30.

81 Vigl B, Aebischer D, Nitschké M, *et al.* Tissue inflammation modulates gene expression of lymphatic endothelial cells and dendritic cell migration in a stimulus-dependent manner. *Blood* 2011; **118**: 205–15.

82 Nourshargh S, Hordijk PL, Sixt M. Breaching multiple barriers: leukocyte motility through venular walls and the interstitium. 2010. DOI:10.1038/nrm2889.

83 Hubbard AK, Rothlein R. Intercellular adhesion molecule-1 (ICAM-1) expression and cell signaling cascades. *Free Radic Biol Med* 2000; **28**: 1379–86.

84 Sundd P, Pospieszalska MK, Cheung S-L, Konstantopoulos K, Ley K. Biomechanics of leukocyte rolling. DOI:10.3233/BIR-2011-0579.

85 Habashi JP, Doyle JJ, Holm TM, *et al.* Angiotensin II Type 2 Receptor Signaling Attenuates Aortic Aneurysm in Mice Through ERK Antagonism. *Science (80-)* 2011; **332**: 361–5.

86 Mu H, Wang X, Lin P, Yao Q, Chen C. Nitrotyrosine promotes human aortic smooth

muscle cell migration through oxidative stress and ERK1/2 activation. *Biochim Biophys Acta - Mol Cell Res* 2008; **1783**: 1576–84.

87 Gaut JP, Byun J, Tran HD, *et al.* Myeloperoxidase produces nitrating oxidants in vivo. *J Clin Invest* 2002; **109**: 1311–9.

88 Sabatier L, Chen D, Fagotto-Kaufmann C, *et al.* Fibrillin Assembly Requires Fibronectin. *Mol Biol Cell* 2009; **20**: 846–58.

89 Wong ND, Gransar H, Narula J, *et al.* Myeloperoxidase, Subclinical Atherosclerosis, and Cardiovascular Disease Events. *JACC Cardiovasc Imaging* 2009; **2**: 1093–9.

90 Vita JA, Brennan M-L, Gokce N, *et al.* Serum Myeloperoxidase Levels Independently Predict Endothelial Dysfunction in Humans. *Circulation* 2004; **110**: 1134–9.

91 Bui TM, Wiesolek HL, Sumagin R. ICAM-1: A master regulator of cellular responses in inflammation, injury resolution, and tumorigenesis. *J Leukoc Biol* 2020; **108**: 787–99.

92 Stocker R, Huang A, Jeranian E, *et al.* Hypochlorous Acid Impairs Endothelium-Derived Nitric Oxide Bioactivity Through a Superoxide-Dependent Mechanism. *Arterioscler Thromb Vasc Biol* 2004; **24**: 2028–33.

93 Eiserich JP, Baldus S, Brennan M-L, *et al.* Myeloperoxidase, a Leukocyte-Derived Vascular NO Oxidase. *Science (80-)* 2002; **296**: 2391–4.

94 Cheng D, Talib J, Stanley CP, *et al.* Inhibition of MPO (Myeloperoxidase) Attenuates Endothelial Dysfunction in Mouse Models of Vascular Inflammation and Atherosclerosis. *Arterioscler Thromb Vasc Biol* 2019; **39**: 1448–57.

95 Mehrkens D, Nettersheim FS, Ballmann F, *et al.* Inhibition of myeloperoxidase attenuates thoracic aortic aneurysm formation in Marfan disease. *bioRxiv* 2022. DOI:10.1101/2022.11.24.517172.

96 Groenink M, den Hartog AW, Franken R, *et al.* Losartan reduces aortic dilatation rate in adults with Marfan syndrome: a randomized controlled trial. *Eur Heart J* 2013; **34**: 3491–500.

97 Chiu H-H, Wu M-H, Wang J-K, *et al.* Losartan Added to β-Blockade Therapy for Aortic Root Dilation in Marfan Syndrome: A Randomized, Open-Label Pilot Study. *Mayo Clin Proc* 2013; **88**: 271–6.

98 Verhagen JMA, Burger J, Bekkers JA, *et al.* Multi-omics profiling in marfan syndrome: Further insights into the molecular mechanisms involved in aortic disease. *Int J Mol Sci* 2022; **23**: 438.

99 Lim W-W, Dong J, Ng B, *et al.* Inhibition of IL11 Signaling Reduces Aortic Pathology in Murine Marfan Syndrome. *Circ Res* 2022; **130**: 728–40.

100 Guido MC, Lopes N de M, Albuquerque CI, *et al.* Treatment With Methotrexate Associated With Lipid Core Nanoparticles Prevents Aortic Dilation in a Murine Model of Marfan Syndrome. *Front Cardiovasc Med* 2022; **9**. DOI:10.3389/fcvm.2022.893774.

101 Ndrepepa G. Myeloperoxidase – A bridge linking inflammation and oxidative stress with cardiovascular disease. *Clin Chim Acta* 2019; **493**: 36–51.

102 Ágg B, Szilveszter B, Daradics N, *et al.* Increased visceral arterial tortuosity in Marfan syndrome. *Orphanet J Rare Dis* 2020; **15**: 91.

103 Inghardt T, Antonsson T, Ericsson C, *et al.* Discovery of AZD4831, a Mechanism-Based Irreversible Inhibitor of Myeloperoxidase, As a Potential Treatment for Heart Failure with Preserved Ejection Fraction. *J Med Chem* 2022; **65**: 11485–96.

7. Attachments

7.1. Figures

7.2. Tables

8. Previously published results

Published as preprint and currently under revision at Cardiovascular Research and Arteriosclerosis, Thrombosis, and Vascular Biology.[95]